HHS Public Access

Author manuscript

ACS Chem Neurosci. Author manuscript; available in PMC 2017 February 17.

Published in final edited form as:

ACS Chem Neurosci. 2016 February 17; 7(2): 218–226. doi:10.1021/acschemneuro.5b00280.

Opposing Effects of Cucurbit[7]uril and 1,2,3,4,6-penta-O-galloyl-β-D-glucopyranose on Amyloid $\beta_{25–35}$ Assembly

Natália E. C. de Almeida[†], **Thanh D. Do**[†,¥], **Michael Tro**[†], **Nichole E. LaPointe**[‡], **Stuart C. Feinstein**[‡], **Joan-Emma Shea**[†], and **Michael T. Bowers**[†,*]

[†]Department of Chemistry and Biochemistry, University of California, Santa Barbara, California 93106, United States

[‡]Neuroscience Research Institute and Department of Molecular Cellular and Developmental Biology, University of California, Santa Barbara, California 93106, United States

Abstract

Alzheimer's disease (AD) is a neurodegenerative disease characterized by extracellular deposits of amyloid β-protein (Aβ) in the brain. The conversion of soluble monomers to amyloid Aβ fibrils is a complicated process and involves several transient oligomeric species, which are widely believed to be highly toxic and play a crucial role in the etiology of AD. The development of inhibitors to prevent formation of small and mid-sized oligomers is a promising strategy for AD treatment. In this work, we employ ion mobility spectrometry (IMS), transmission electron microscopy (TEM) and molecular dynamics (MD) simulations to elucidate the structural modulation promoted by two potential inhibitors of Aβ oligomerization, cucurbit[7]uril (CB[7]) and 1,2,3,4,6-penta-O-galloyl-β-D-glucopyranose (PGG), on early oligomer and fibril formation of the A$\beta_{25–35}$ fragment. One and two CB[7] molecules bind to A$\beta_{25–35}$ monomers and dimers, respectively, and suppress aggregation by remodeling early oligomer structures and inhibiting the formation of higher-order oligomers. On the other hand, non-selective binding was observed between PGG and A$\beta_{25–35}$. The interactions between PGG and A$\beta_{25–35}$, surprisingly, enhanced the formation of Aβ aggregates by promoting extended A$\beta_{25–35}$ conformations in both homo- and hetero-oligomers. When both ligands were present, the inhibitory effect of CB[7] overrode the stimulatory effect of PGG on A$\beta_{25–35}$ aggregation, suppressing the formation of large amyloid oligomers and eliminating the structural conversion from isotropic to β-rich topologies induced by PGG. Our results provide mechanistic insights into CB[7] and PGG action on Aβ oligomerization.

[*]Corresponding author: Michael T. Bowers. Tel: +1-805-893-2673; bowers@chem.ucsb.edu.

[¥]Department of Chemistry and the Beckman Institute, University of Illinois at Urbana-Champaign, Urbana, Illinois 61801, United States.

Author Contributions

N.E.C.A. and T.D.D. contributed equally.

Notes

The authors declare no competing financial interest.

Supporting Information. Detailed description of materials and methods, sample preparation, ion mobility spectrometry coupled mass spectrometry (IMS-MS), transmission electron microscopy (TEM), molecular dynamic (MD) simulations and cross section calculations. Mass spectra, arrival time distributions (ATDs) and TEM images of pure A$\beta_{25–35}$ sample and in the presence of cucurbit[7]uril (CB[7]) and 1,2,3,4,6-penta-O-galloyl-β-D-glucopyranose (PGG). This information is available free of charge via the Internet at http://pubs.acs.org.

They also demonstrate the power of the IMS technique to investigate mechanisms of multiple small-molecule agents on the amyloid formation process.

Keywords

amyloids; polyphenols; cucurbiturils; ion-mobility mass spectrometry; computational modeling; amyloid-β

INTRODUCTION

Alzheimer's disease (AD) is a neurodegenerative disease pathologically characterized by extracellular deposits of amyloid β-protein (Aβ) in the brain, resulting in neuronal cell loss and subsequent dementia.[1–6] However, the toxicity of Aβ is not mediated by these large aggregates of Aβ. Rather, neurotoxicity correlates with the rapid self-assembly of soluble, oligomeric forms of Aβ. Interestingly, there are two major forms of Aβ: A$\beta_{1–42}$ constitutes only ~9 % of the total Aβ in the brain and is the more toxic alloform, whereas the more abundant species A$\beta_{1–40}$ (~90 %) is less toxic and has a slower aggregation rate.[7–11] The conversion of soluble Aβ monomers to amyloid Aβ fibrils is a complicated, dynamic process involving several transient oligomeric species,[12–17] several of which appear to be highly toxic and play a crucial role in the development of AD.[18,19]

Although there are presently no effective treatments for AD, several therapeutic strategies are under development for prevention and treatment.[20–25] Approaches based on suppressing Aβ fibril formation appear to be insufficient and are likely to be unsuccessful given that soluble oligomers, rather than fibrils, are the probable toxic agents.[14,26,27] In this context, the search for potential inhibitors to shorten the lifetime of small and mid-sized oligomers has attracted great attention.[25,28–32] Promising results have been reported employing polyphenol derivatives as inhibitors of amyloid formation.[30,31,33–35] In particular, 1,2,3,4,6-penta-O-galloyl-β-D-glucopyranose (PGG) (see Scheme 1), a large polyphenol from the traditional medicinal herb *Paeonia suffruticosa*, was reported to be a potent inhibitor for the aggregation of both A$\beta_{1–40}$ and A$\beta_{1–42}$.[33] However, it is unclear whether there are specific interaction motifs between polyphenols and amyloid peptides, as these compounds tend to form complexes with a wide range of proteins and peptides including Aβ, islet amyloid polypeptide (IAPP), α-synuclein, and tau.[30,34,36,37] It has been suggested that the inhibitory mechanism of polyphenols may be size and shape-dependent. For example, a previous study has shown that epigallocatechin gallate (EGCG; a polyphenol extracted from green tea) is an effective inhibitor of A$\beta_{25–35}$ aggregation because the peptide can tightly wrap around three faces of the inhibitor, whose shape resembles a propeller.[31] Another study has shown that the effects of inositols, a class of small polyphenols, on amyloid aggregation are stereochemistry dependent.[38] However, there is not enough evidence to correlate inhibitory effects with the shapes of the polyphenols and the lengths of the peptide targets.

Recently, a new supramolecular strategy approach has been employed to target certain types of residues explicitly.[32,39–41] For example, cucurbit[7]uril (CB[7]) (see Scheme 1), a synthetic macrocyclic receptor molecule,[42–44] has demonstrated inhibitory effects by locking aromatic residues inside its hollow core.[40] Each cucurbituril possesses a rigid

hydrophobic cavity lying between the two oxygen-atom-rich rims, making it a compatible structure for host-guest chemistry.[45] The inhibitory effect of CB[7] on Aβ aggregation was suggested to be associated primarily with its hydrophobic cavity capable of capturing aromatic residues.[46] Polar and charged residues can in principle also interact with the hydrophilic surfaces of the molecule, but there is currently lack of experimental support for this effect.

The mechanistic effect of ligands like PGG and CB[7], individually or in combination, on transient early-stage soluble Aβ oligomers is unknown. Here, we investigate the effect of these ligands on oligomer and fibril formation of A$\beta_{25–35}$ (see Scheme 1), a cytotoxic fragment of Aβ that has been studied extensively by experimental and computational techniques.[31,47–54] The transient and polymorphic nature of aggregating systems poses significant challenges for traditional techniques aimed at detecting and characterizing early oligomer formation. Ion mobility spectrometry coupled mass spectrometry (IMS-MS) overcomes many of these challenges, and has been applied successfully to studies of structural changes in the self-assembly of Aβ and similar systems,[14,55,56] as well as to the evaluation of small-molecules that interfere with the Aβ assembly process.[29,31,32,57–60] We report herein the effects of CB[7] and PGG on oligomer formation and aggregate morphologies of A$\beta_{25–35}$ using IMS-MS, transmission electron microscopy (TEM), and molecular dynamics (MD) simulations.

RESULTS and DISCUSSION

A$\beta_{25–35}$ aggregation and the transition of oligomeric states from isotropic to β-sheet

The nano-ESI-Q mass spectrum of A$\beta_{25–35}$ is given in Figure 1A. Numerous peaks are reported with respect to their n/z ratios, where n is the oligomer number and z the charge, including n/z = 1/2 (m/z = 530) and n/z = 1/1 (m/z = 1060) and numerous less intense peaks for higher order oligomers. Since these are relatively low resolution spectra a given n/z can contain several oligomeric states. For example n/z = 1/1 can also be n/z = 2/2. The various contributions of different oligomeric states to each peak can be obtained from the arrival time distributions (ATDs) given in Figure S2 in Supporting Information.

The experimental collisional cross sections (CCS) (reported in Figures 2A and Supporting Information, Figure S2 and Table S1) are obtained from measuring ATDs at different pressure to voltage (P/V) ratios from a plot of arrival time (t_A) versus P/V (Equations S3 and S4). To analyze the transient states of the soluble oligomers, the experimental data were compared to the ideal isotropic growth model (Figure 2), in which the isotropic growth approximates the cross section of an oligomer whose structure is equally distributed in all spatial dimensions ($\sigma_n = \sigma_1 \times n^{2/3}$).[31,61] For A$\beta_{25–35}$ a positive deviation from the ideal isotropic growth model is observed at the dimer and increasingly significant deviations are observed for trimers and larger oligomeric species (Figure 2A). Recent studies[31,61,62] have convincingly shown that significant and persistent positive deviations of oligomers above the isotropic growth curve are reliable indicators of β-sheet formation. This occurs because β-sheet growth occurs in a linear manner and hence the CCSs of β-sheet oligomers increase linearly with n, the oligomer number, not as $n^{2/3}$ which describes isotropic growth. More specifically, previous work has shown that the formation of β-sheet-like trimers and

tetramers is a crucial step in the process of A$\beta_{25–35}$ aggregation.[31,47,63] In summary, the IMS-MS data indicate that extended β-sheet conformations are populated more abundantly as the A$\beta_{25–35}$ oligomer number increases, a clear signature of eventual amyloid fibril formation. These results are consistent with TEM images (Figure 3A) that shows the formation of amyloid fibrils and were obtained from the same A$\beta_{25–35}$ sample used in the IMS-MS experiments. Our data here are also consistent with previous studies on the same system.[31]

Inhibitory effect of cucurbit[7]uril (CB[7]) on A$\beta_{25–35}$ amyloid aggregation

As shown in Figures 1B and 2B, the presence of an equimolar concentration of CB[7] remodels and dramatically reduces the steady-state oligomer distribution of A$\beta_{25–35}$. In the presence of CB[7], the only identified A$\beta_{25–35}$ homo-oligomers are monomers at n/z = 1/2 (m/z = 530) and n/z = 1/1 (m/z = 1060), dimer at n/z = 2/2 (m/z = 1060), trimer at n/z = 3/4 (m/z = 795) and hexamers at n/z = 6/7 (m/z = 908) and n/z = 6/11 (m/z = 578). The low charge state mass spectral peaks at high m/z are absent, indicating that CB[7] not only modulated oligomer structures (see discussion below), but also prevented the formation of large oligomers.

Two new mass spectral peaks are recognized in Figure 1B as A$\beta_{25–35}$:CB[7] hetero-oligomers, in which the most abundant peak at m/z = 741 is a triply charged heterodimer of an A$\beta_{25–35}$ monomer and one CB[7] molecule (($n+k$)/z = (1+1)/3), where k is the number of CB[7] molecules, and the peak at m/z = 1111 is a doubly charged heterodimer (see Figure S3 and Table S2). The CCSs obtained for A$\beta_{25–35}$:CB[7] hetero-oligomers (Figure 4A) suggest that the dimer is globular but the monomer has two conformations, one globular and one extended conformer.

At 1:10 A$\beta_{25–35}$:CB[7] molar ratio, there are only three remaining homo-oligomers: A$\beta_{25–35}$ monomers and dimers at n/z = 1/2 (m/z = 530), n/z = 1/1 (m/z = 1060) and n/z = 2/2 (m/z = 1060) (Figure S1). The remaining peaks are A$\beta_{25–35}$:CB[7] hetero complexes previously described. The higher intensities of these A$\beta_{25–35}$:CB[7] complex peaks at 1:10 ratio suggests that CB[7] competitively binds to A$\beta_{25–35}$ species and suppresses A$\beta_{25–35}$ oligomer growth. Our data indicate that CB[7] is a very effective inhibitor that intervenes in the aggregation cascade by blocking self-assembly at the dimer stage. TEM imaging (Figures 3B, C) shows that CB[7] reduces the formation of macroscopic fibrillar aggregates compared to the TEM image of the pure A$\beta_{25–35}$, supporting the IMS-MS data.

Computational modeling provides evidence supporting an inhibitory effect of CB[7] on the amyloid formation of A$\beta_{25–35}$. The simulations reveal that CB[7] ligands preferentially capture the amino-groups of lysines (Lys28), and to a lesser extent, the positively charged N-termini of A$\beta_{25–35}$ monomers (see Figure 5). The binding of CB[7] specifically to lysines is also observed with the 38-residue islet amyloid polypeptide whose aggregation is a pathological hallmark of Type 2 Diabetes.[41] The interaction motif is similar to the molecular tweezer ligands that possess torus-shaped binding pockets.[32,64,65] The polar pockets serve as specific hosts for charged residues, and the strong binding between protein:ligand complexes can modulate the aggregation cascade. Each CB[7] molecule has only one

binding site for A$\beta_{25–35}$ and the bulkiness of CB[7] helps to isolate the A$\beta_{25–35}$ monomers from each other and prevent large oligomer formation.

1,2,3,4,6-penta-O-galloyl-β-D-glucopyranose (PGG) enhances A$\beta_{25–35}$ amyloid aggregation

In the mass spectrum of A$\beta_{25–35}$ incubated with PGG at a 1:1 molar ratio (Figure 1C) significant homo- and hetero-oligomers are present. This is in contrast to the mixture of A$\beta_{25–35}$ with CB[7] where very few oligomers are observed. The CCS data (Figures 2C and 4B, and Supporting Information, Figure S4 and Table S3) indicate the formation of extended A$\beta_{25–35}$ homo-oligomers and A$\beta_{25–35}$:PGG hetero-oligomers, which correlates with a conformational conversion from isotropic to β-sheet structures. It has been previously shown that the conformational transition of A$\beta_{25–35}$ trimer and tetramer from native to β-sheet is a crucial step for A$\beta_{25–35}$ fibril formation.[31,47] Therefore we examined the ATDs of the mass spectral peaks corresponding to these oligomers in the presence of PGG. The ATD at 795 *m/z* for the pure A$\beta_{25–35}$ sample displays only a compact trimer at ~0.51 ms (Figure 6A). However, the ATD of the same *m*/*z* in the A$\beta_{25–35}$:PGG mixture shows two distinct features corresponding to a compact structure (at ~0.51 ms) and a new dominant feature for an extended trimer at ~0.58 ms (Figure 6B). For the A$\beta_{25–35}$ tetramer (*n*/*z* = 4/3) at *m*/*z* = 1413, the ATDs show two features for both A$\beta_{25–35}$ and A$\beta_{25–35}$:PGG (Figure 6C, D), however, there is an increase in the population of the extended species when the ligand is added. The enhanced formation of extended Aβ trimers and tetramers in the presence of PGG unambiguously demonstrates that the ligand facilitates the conformational transition of A$\beta_{25–35}$ oligomers from compact to extended. This result is very surprising and intriguing because PGG was originally thought to be an amyloid inhibitor.[33,35] The TEM images (Figure 3D, E) of the same samples used in IMS-MS experiments show a concentration-dependent increase in the abundance of fibrillar A$\beta_{25–35}$ aggregates in the presence of PGG. The fibrils in the mixed system show a twisted morphology, whereas the fibrils obtained from the pure A$\beta_{25–35}$ sample showed a combination of straight and twisted morphologies. Lastly, the fibrils become more abundant in the presence of *excess* PGG (1:10 ratio), further suggesting that this ligand is not an aggregation inhibitor for A$\beta_{25–35}$, but rather an aggregation accelerator.

The MD simulations provide insight into A$\beta_{25–35}$ behavior in the presence of PGG. Since PGG is a large polyphenol, A$\beta_{25–35}$ is unable to wrap around this molecule like it could with EGCG (Figure 7).[31] Unlike the case of CB[7], there are no specific binding sites between the ligand and peptide. The PGG core formed by one or more ligand molecules provides a template surface with both hydrophobic and hydrophilic sites to which one or more amphipathic A$\beta_{25–35}$ peptides can weakly attach and undergo structural conversion. This observation from the MD simulations is consistent with the experimental detection of complexes made of multiple PGG molecules and A$\beta_{25–35}$ in which the A$\beta_{25–35}$ oligomers adopt extended conformations. Lastly, the theoretical cross sections of hetero-oligomers extracted from the simulation show good agreement with experimental data.

Cucurbit[7]uril (CB[7]) overrides the effect of 1,2,3,4,6-penta-O-galloyl-β-D-glucopyranose (PGG) on A$\beta_{25–35}$ amyloid aggregation

Interestingly, when fresh A$\beta_{25–35}$ peptide is incubated together with both PGG and CB[7] at a 1:1:1 molar ratio, most A$\beta_{25–35}$ homo-oligomers become depleted (Figures 1D and 2D) and A$\beta_{25–35}$:CB[7] complexes dominate. No A$\beta_{25–35}$:PGG complexes are found in the mass spectrum. Instead, two new peaks appear at m/z = 791 and m/z = 845, which are accounted for by the "triple" complexes formed from A$\beta_{25–35}$, PGG and CB[7] molecules (i.e., $(n+p+k)/z$ = (1+1+1)/4 and (2+1+1)/5), respectively).

The dominance of binary complexes between A$\beta_{25–35}$ and CB[7] in the 1:1:1 mixture indicates that A$\beta_{25–35}$ forms more stable complexes with CB[7] than with PGG. In addition, the formation of triple complexes between the peptide and the two ligands is intriguing. From the cross section data (Figure S5 and Table S4), the hetero-oligomer topologies are consistent with an isotropic conformation (Figure 4C). The data indicate that the strong inhibitory effect of CB[7] overrides the conformational conversion from isotropic to β-sheet structures and the multimeric A$\beta_{25–35}$ homo-oligomer formation promoted by the polyphenol. In a good agreement with the IMS-MS results, the TEM imaging in the presence of both CB[7] and PGG (Figure 3F) shows the formation of globular aggregates, and very few short and irregular fibers (data not shown).

In a further experiment, CB[7] was added to an A$\beta_{25–35}$ sample previously incubated with PGG (for 1 week at 1:1 ratio) to give final molar ratios of 1:1:5 and 1:1:10 of A$\beta_{25–35}$:PGG:CB[7], and the samples were incubated an additional two days. The TEM images (Figure S6) indicate that addition of CB[7] to the aged A$\beta_{25–35}$:PGG sample reduces the amount of fibrillar aggregates. Although some of the remaining fibers retain a typical amyloid fiber morphology, most exhibit some degree of irregularity, with regions that are thicker and more heavily stained. Indeed, the irregular fibers were similar to those few fibers that were observed when PGG and CB[7] were both present from the onset of aggregation (not shown). Collectively, these results demonstrate that CB[7] inhibits the assembly of fibrillar A$\beta_{25–35}$ aggregates and also triggers their disassembly in a concentration-dependent manner.

SUMMARY and CONCLUSIONS

In the current study, IMS-MS data reveal distinctive effects of two assembly modulators, CB[7] and PGG, on the amyloid aggregation system, as well as on the structures of A$\beta_{25–35}$ homo- and hetero-oligomers. The self-assembly of pure A$\beta_{25–35}$ (Figures 1A, 2A) proceeds from compact monomers into β-rich oligomers emerging at the dimer and trimer stages. In the presence of CB[7], one and two CB[7] molecules selectively bind to A$\beta_{25–35}$ monomer and dimer, respectively. The most probable binding site for CB[7] on A$\beta_{25–35}$ is the lysine residue (Lys28). This observation expands our knowledge of the action mechanism of CB[7], since its inhibitory effect on β-amyloid fibrillation was previously understood to involve the capture of only aromatic residues: The hydrophilic rims of CB[7] created by oxygen atoms are a potential site to capture polar and charged residues, while the hydrophobic cavity hosts aromatic residues. These two possible host sites reveal the versatility of CB[7] as a possible novel therapeutic agent for AD. The IMS-MS data reveal

that CB[7] suppresses A$\beta_{25–35}$ aggregation by preventing homo-oligomer formation. Complex formation between CB[7] and A$\beta_{25–35}$ monomers and dimers depletes the population of A$\beta_{25–35}$ oligomers larger than dimer. Consequently, fewer fibrillar A$\beta_{25–35}$ aggregates are found by TEM imaging at a 1:1 A$\beta_{25–35}$:CB[7] molar ratio and aggregates are only very rarely observed at a 1:10 A$\beta_{25–35}$:CB[7] ratio (Figure 3B, C).

In contrast to CB[7], PGG significantly enhances the formation of A$\beta_{25–35}$ aggregates (Figures 1C, 2C and 4B). Complex formation between PGG and A$\beta_{25–35}$ promotes extended A$\beta_{25–35}$ conformations in both homo- and hetero-oligomers (Figures 6 and 7). Consequently, long fibrillar A$\beta_{25–35}$ aggregates are found by TEM in the presence of PGG at a 1:1 A$\beta_{25–35}$:PGG ratio, and these become remarkably more abundant with an increase in PGG molar ratio (1:10 of A$\beta_{25–35}$:PGG) (Figure 3D, E). This is the first time a polyphenol has been shown to accelerate amyloid formation. These experimental results diverge from previous reports in the literature,[33] which describe a strong inhibitory effect of PGG on the fibril formation of A$\beta_{1–40}$ and A$\beta_{1–42}$ (of which A$\beta_{25–35}$ is a fragment). The chemical structure of PGG possesses both hydrophobic (aromatic rings) and hydrophilic (hydroxyl groups) sites for Aβ binding. In fact, both IMS-MS and MD data indicate that the binding of this ligand to the peptide is non-selective. The opposing effects of PGG on A$\beta_{25–35}$ and full-length A$\beta_{1–40}$/A$\beta_{1–42}$ may arise from the difference in the conformations required for aggregation. Short peptides such as A$\beta_{25–35}$ can aggregate when adopting extended conformations[31,47] whereas the monomers of A$\beta_{1–40}$/A$\beta_{1–42}$ in the fibril state exist in strand-loop-strand conformations.[66,67] Another possibility is that PGG suppresses fibril formation in A$\beta_{1–40}$/A$\beta_{1–42}$ by interacting with segments other than A$\beta_{25–35}$. A$\beta_{16–22}$ [KLVFFAE][68] could be a probable target for PGG as it contains an important hydrophobic stretch and aromatic residues that can interact with PGG through π-stacking.

Finally, when both CB[7] and PGG are simultaneously present during aggregation, the dominance of binary complexes of A$\beta_{25–35}$ and CB[7] over A$\beta_{25–35}$ and PGG indicates that the inhibitory effect of CB[7] overrides the stimulatory effect of PGG (Figures 1D, 2D and 4C). CB[7] competitively binds to not only A$\beta_{25–35}$ homo-oligomers, but also hetero-A$\beta_{25–35}$:PGG complexes, thereby suppressing the formation of large A$\beta_{25–35}$ oligomers and eliminating the isotropic to β-rich structural conversion induced by PGG.

METHODS

A detailed description of materials and methods is given in Supporting Information (Section S1). The stock solutions were prepared as follows: A$\beta_{25–35}$ and CB[7] samples were prepared in acidified water (0.1% (v/v) formic acid), whereas PGG was dissolved in water containing 20% methanol (v/v). These stock solutions were used for all experiments (pure A$\beta_{25–35}$, A$\beta_{25–35}$ with CB[7], A$\beta_{25–35}$ with PGG and A$\beta_{25–35}$ with PGG and CB[7] samples). For IMS-MS analysis, the samples were loaded into gold coated nano-ESI capillaries and electrosprayed in a home-built ion mobility spectrometry-mass spectrometer.[69] The theoretical cross sections were calculated using the projected superposition approximation (PSA) method available at http://luschka.bic.ucsb.edu:8080/WebPSA/.[70,71] For the TEM analyses, aliquots of the same sample solutions used in IMS-

MS experiments were adsorbed onto mesh formvar/carbon copper grids and imaged on a JEOL 123 microscope with an ORCA camera and AMT Image Capture Software v. 5.24.

Supplementary Material

Refer to Web version on PubMed Central for supplementary material.

Acknowledgments

N.E.C.A. thanks Conselho Nacional de Desenvolvimento Científico e Tecnológico (CNPq) for a post doctoral fellowship (204613/2014-0). We gratefully acknowledge support from the National Science Foundation (NSF) Grants CHE-1301032 (M.T.B.) and MCB-1158577 (J.-E.S.), the National Institutes of Health Grant 1RO1AG047116-01 (M.T.B.), the David and Lucile Packard Foundation (J.-E.S.), and a grant from Santa Barbara Cottage Hospital and the University of California, Santa Barbara (N.E.L). This work used the Extreme Science and Engineering Discovery Environment (XSEDE), which is supported by National Science Foundation Grant OCI-1053575. We acknowledge the Texas Advanced Computing Center (TACC) at the University of Texas at Austin for providing HPC resources through XSEDE Grant TG-MCA05S027 (J.- E.S.), and the NRI Microscopy Facility at UCSB. We acknowledge support from the Center for Scientific Computing at the CNSI and MRL via NSF MRSEC (DMR-1121053) and NSF Grant CNS-0960316.

ABREVIATIONS USED

AD	Alzheimer's disease
Aβ	amyloid β-protein
A$\beta_{1–40}$	amyloid β-protein (1–40)
A$\beta_{1–42}$	amyloid β-protein (1–42)
A$\beta_{25–35}$	amyloid β-protein (25–35)
A$\beta_{16–22}$	amyloid β-protein (16–22)
ATD	arrival time distribution
CB[7]	cucurbit[7]uril
CCS	collision cross sections
EGCG	epigallocatechin gallate
IAPP	islet amyloid polypeptide
IMS	ion mobility spectrometry
IMS-MS	ion mobility spectrometry coupled mass spectrometry
Lys	lysines
MD	molecular dynamics
PGG	1,2,3,4,6-penta-O-galloyl-β-D-glucopyranose
t_A	arrival time
TEM	transmission electron microscopy

References

1. Hardy J, Selkoe DJ. The amyloid hypothesis of Alzheimer's disease: progress and problems on the road to therapeutics. Science. 2002; 297:353–356. [PubMed: 12130773]
2. Lee HG, Zhu XW, Castellani RJ, Nunomura A, Perry G, Smith MA. Amyloid-β in Alzheimer disease: the null versus the alternate hypotheses. J Pharm Exper Ther. 2007; 321:823–829.
3. Karran E, Mercken M, De Strooper B. The amyloid cascade hypothesis for Alzheimer's disease: an appraisal for the development of therapeutics. Nat Rev Drug Discov. 2011; 10:698–U1600. [PubMed: 21852788]
4. Zaghi J, Goldenson B, Inayathullah M, Lossinsky AS, Masoumi A, Avagyan H, Mahanian M, Bernas M, Weinand M, Rosenthal MJ, Espinosa-Jeffrey A, de Vellis J, et al. Alzheimer disease macrophages shuttle amyloid-β from neurons to vessels, contributing to amyloid angiopathy. Acta Neuropathol. 2009; 117:111–124. [PubMed: 19139910]
5. Jakob-Roetne R, Jacobsen H. Alzheimer's disease: from pathology to therapeutic approaches. Angew Chem Int Ed Engl. 2009; 48:3030–3059. [PubMed: 19330877]
6. Tanzi RE, Bertram L. Twenty years of the Alzheimer's disease amyloid hypothesis: a genetic perspective. Cell. 2005; 120:545–555. [PubMed: 15734686]
7. Lambert MP, Barlow AK, Chromy BA, Edwards C, Freed R, Liosatos M, Morgan TE, Rozovsky I, Trommer B, Viola KL, Wals P, Zhang C, et al. Diffusible, nonfibrillar ligands derived from Aβ1–42 are potent central nervous system neurotoxins. Proc Natl Acad Sci U S A. 1998; 95:6448–6453. [PubMed: 9600986]
8. Hasegawa K, Yamaguchi I, Omata S, Gejyo F, Naiki H. Interaction between Aβ(1–42) and Aβ(1–40) in Alzheimer's β-amyloid fibril formation in vitro. Biochemistry. 1999; 38:15514–15521. [PubMed: 10569934]
9. Jarrett JT, Berger EP, Lansbury PT. The carboxy terminus of the β-amyloid protein is critical for the seeding of amyloid formation - implications for the pathogenesis of Alzheimers-disease. Biochemistry. 1993; 32:4693–4697. [PubMed: 8490014]
10. Kuperstein I, Broersen K, Benilova I, Rozenski J, Jonekheere W, Debulpaep M, Vandersteen A, Segers-Nolten I, Van der Werf K, Subramaniam V, Braeken D, Callewaert G, et al. Neurotoxicity of Alzheimer's disease Aβ peptides is induced by small changes in the Aβ42 to Aβ40 ratio. EMBO J. 2010; 29:3408–3420. [PubMed: 20818335]
11. Haass C, Selkoe DJ. Soluble protein oligomers in neurodegeneration: lessons from the Alzheimer's amyloid β-peptide. Nat Rev Mol Cell Biol. 2007; 8:101–112. [PubMed: 17245412]
12. Chiti F, Dobson CM. Amyloid formation by globular proteins under native conditions. Nat Chem Biol. 2008; 5:15–21. [PubMed: 19088715]
13. Krafft GA, Klein WL. ADDLs and the signaling web that leads to Alzheimer's disease. Neuropharmacology. 2010; 59:230–242. [PubMed: 20650286]
14. Bernstein SL, Dupuis NF, Lazo ND, Wyttenbach T, Condron MM, Bitan G, Teplow DB, Shea JE, Ruotolo BT, Robinson CV, Bowers MT. Amyloid-β protein oligomerization and the importance of tetramers and dodecamers in the aetiology of Alzheimer's disease. Nat Chem. 2009; 1:326–331. [PubMed: 20703363]
15. Teplow DB, Lazo ND, Bitan G, Bernstein S, Wyttenbach T, Bowers MT, Baumketner A, Shea JE, Urbanc B, Cruz L, Borreguero J, Stanley HE. Elucidating amyloid β–protein folding and assembly: a multidisciplinary approach. Acc Chem Res. 2006; 39:635–645. [PubMed: 16981680]
16. Eisenberg D, Nelson R, Sawaya MR, Balbirnie M, Sambashivan S, Ivanova MI, Madsen AO, Riekel C. The structural biology of protein aggregation diseases: fundamental questions and some answers. Acc Chem Res. 2006; 39:568–575. [PubMed: 16981672]
17. Eisenberg D, Jucker M. The amyloid state of proteins in human diseases. Cell. 2012; 148:1188–1203. [PubMed: 22424229]
18. Ono K, Condron MM, Teplow DB. Structure-neurotoxicity relationships of amyloid β-protein oligomers. Proc Natl Acad Sci U S A. 2009; 106:14745–14750. [PubMed: 19706468]
19. Noguchi A, Matsumura S, Dezawa M, Tada M, Yanazawa M, Ito A, Akioka M, Kikuchi S, Sato M, Ideno S, Noda M, Fukunari A, et al. Isolation and characterization of patient-derived, toxic,

high mass amyloid β-protein (Aβ) assembly from Alzheimer disease brains. J Biol Chem. 2009; 284:32895–32905. [PubMed: 19759000]

20. Estrada LD, Soto C. Disrupting β-amyloid aggregation for Alzheimer disease treatment. Curr Top Med Chem. 2007; 7:115–126. [PubMed: 17266599]
21. Bates KA, Verdile G, Li QX, Ames D, Hudson P, Masters CL, Martins RN. Clearance mechanisms of Alzheimer's amyloid-β peptide: implications for therapeutic design and diagnostic tests. Mol Psychiatry. 2009; 14:469–486. [PubMed: 18794889]
22. Mason JM, Kokkoni N, Stott K, Doig AJ. Design strategies for anti-amyloid agents. Curr Opin Struc Biol. 2003; 13:526–532.
23. Bartolini M, Andrisano V. Strategies for the inhibition of protein aggregation in human diseases. ChemBioChem. 2010; 11:1018–1035. [PubMed: 20401887]
24. Liu TY, Bitan G. Modulating self-assembly of amyloidogenic proteins as a therapeutic approach for neurodegenerative diseases: strategies and mechanisms. ChemMedChem. 2012; 7:359–374. [PubMed: 22323134]
25. Feng BY, Toyama BH, Wille H, Colby DW, Collins SR, May BCH, Prusiner SB, Weissman J, Shoichet BK. Small-molecule aggregates inhibit amyloid polymerization. Nat Chem Biol. 2008; 4:197–199. [PubMed: 18223646]
26. Ahmed M, Davis J, Aucoin D, Sato T, Ahuja S, Aimoto S, Elliott JI, Nostrand WEV, Smith SO. Structural conversion of neurotoxic amyloid-β1–42 oligomers to fibrils. Nat Struct Mol Biol. 2010; 17:561–567. [PubMed: 20383142]
27. Stroud JC, Liu C, Teng PK, Eisenberg D. Toxic fibrillar oligomers of amyloid-β have cross-β structure. Proc Natl Acad Sci U S A. 2012; 109:7717–7722. [PubMed: 22547798]
28. McLaurin J, Kierstead ME, Brown ME, Hawkes CA, Lambermon MH, Phinney AL, Darabie AA, Cousins JE, French JE, Lan MF, Chen F, Wong SS, et al. Cyclohexanehexol inhibitors of Aβ aggregation prevent and reverse Alzheimer phenotype in a mouse model. Nat Med. 2006; 12:801–808. [PubMed: 16767098]
29. Zheng X, Gessel MM, Wisniewski ML, Viswanathan K, Wright DL, Bahr BA, Bowers MT. Z-Phe-Ala-diazomethylketone (PADK) disrupts and remodels early oligomer states of the Alzheimer disease Aβ42 protein. J Biol Chem. 2012; 287:6084–6088. [PubMed: 22253440]
30. Ehrnhoefer DE, Bieschke J, Boeddrich A, Herbst M, Masino L, Lurz R, Engemann S, Pastore A, Wanker EE. EGCG redirects amyloidogenic polypeptides into unstructured, off-pathway oligomers. Nat Struc Biol. 2008; 15:558–566.
31. Bleiholder C, Do TD, Wu C, Economou NJ, Bernstein SS, Buratto SK, Shea JE, Bowers MT. Ion mobility spectrometry reveals the mechanism of amyloid formation of Aβ(25–35) and its modulation by inhibitors at the molecular level: epigallocatechin gallate and scyllo-inositol. J Am Chem Soc. 2013; 135:16926–16937. [PubMed: 24131107]
32. Zheng XY, Liu D, Klarner FG, Schrader T, Bitan G, Bowers MT. Amyloid β-protein assembly: the effect of molecular tweezers CLR01 and CLR03. J Phys Chem B. 2015; 119:4831–4841. [PubMed: 25751170]
33. Fujiwara H, Tabuchi M, Yamaguchi T, Iwasaki K, Furukawa K, Sekiguchi K, Ikarashi Y, Kudo Y, Higuchi M, Saido TC, Maeda S, Takashima A, et al. A traditional medicinal herb Paeonia suffruticosa and its active constituent 1,2,3,4,6-penta-O-galloyl-β-D-glucopyranose have potent anti-aggregation effects on Alzheimer's amyloid β proteins in vitro and in vivo. J Neurochem. 2009; 109:1648–1657. [PubMed: 19457098]
34. Porat Y, Abramowitz A, Gazit E. Inhibition of amyloid fibril formation by polyphenols: Structural similarity and aromatic interactions as a common inhibition mechanism. Chem Biol Drug Des. 2006; 67:27–37. [PubMed: 16492146]
35. Bruno E, Pereira C, Roman KP, Takiguchi M, Kao PY, Nogaj LA, Moffet DA. IAPP aggregation and cellular toxicity are inhibited by 1,2,3,4,6-penta-O-galloyl-β-D-glucose. Amyloid. 2013; 20:34–38. [PubMed: 23339420]
36. Palhano FL, Lee J, Grimster NP, Kelly JW. Toward the molecular mechanism(s) by which EGCG treatment remodels mature amyloid fibrils. J Am Chem Soc. 2013; 135:7503–7510. [PubMed: 23611538]

37. Bieschke J, Russ J, Friedrich RP, Ehrnhoefer DE, Wobst H, Neugebauer K, Wanker EE. EGCG remodels mature α-synuclein and amyloid-β fibrils and reduces cellular toxicity. Proc Natl Acad Sci USA. 2010; 107:7710–7715. [PubMed: 20385841]
38. Wang H, Raleigh DP. General amyloid inhibitors? A critical examination of the inhibition of IAPP amyloid formation by inositol stereoisomers. PLoS One. 2014; 9:e104023. [PubMed: 25260075]
39. Yu HJ, Li M, Liu GP, Geng J, Wang JZ, Ren JS, Zhao CQ, Qu XG. Metallosupramolecular complex targeting an α/β discordant stretch of amyloid β peptide. Chem Sci. 2012; 3:3145–3153.
40. Lee HH, Choi TS, Lee SJC, Lee JW, Park J, Ko YH, Kim WJ, Kim K, Kim HI. Supramolecular inhibition of amyloid fibrillation by cucurbit[7]uril. Angew Chem Int Ed. 2014; 53:7461–7465.
41. Lopes DH, Attar A, Nair G, Hayden EY, Du Z, McDaniel K, Dutt S, Bravo-Rodriguez K, Mittal S, Klarner FG, Wang C, Sanchez-Garcia E, et al. Molecular tweezers inhibit islet amyloid polypeptide assembly and toxicity by a new mechanism. ACS Chem Biol. 2015; 10:1555–1569. [PubMed: 25844890]
42. Masson E, Ling XX, Joseph R, Kyeremeh-Mensah L, Lu XY. Cucurbituril chemistry: a tale of supramolecular success. RSC Adv. 2012; 2:1213–1247.
43. Lee JW, Samal S, Selvapalam N, Kim HJ, Kim K. Cucurbituril homologues and derivatives: new opportunities in supramolecular chemistry. Acc Chem Res. 2003; 36:621–630. [PubMed: 12924959]
44. Kim J, Jung IS, Kim SY, Lee E, Kang JK, Sakamoto S, Yamaguchi K, Kim K. New cucurbituril homologues: syntheses, isolation, characterization, and X-ray crystal structures of cucurbit[n]uril (n=5, 7, and 8). J Am Chem Soc. 2000; 122:540–541.
45. Bardelang D, Banaszak K, Karoui H, Rockenbauer A, Waite M, Udachin K, Ripmeester JA, Ratcliffe CI, Ouari O, Tordo P. Probing cucurbituril assemblies in water with TEMPO-like nitroxides: a trinitroxide supraradical with spin-spin interactions. J Am Chem Soc. 2009; 131:5402–5404. [PubMed: 19334727]
46. Lee JW, Lee HHL, Ko YH, Kim K, Kim HI. Deciphering the specific high-affinity binding of cucurbit[7]uril to amino acids in water. J Phys Chem B. 2015; 119:4628–4636. [PubMed: 25757499]
47. Larini L, Shea JE. Role of β-hairpin formation in aggregation: the self-assembly of the amyloid-β(25–35) peptide. Biophys J. 2012; 103:576–586. [PubMed: 22947874]
48. Chang Z, Luo Y, Zhang Y, Wei G. Interactions of Aβ25–35 β-barrel-like oligomers with anionic lipid bilayer and resulting membrane leakage: an all-atom molecular dynamics study. J Phys Chem B. 2011; 115:1165–1174. [PubMed: 21192698]
49. Yu X, Wang Q, Zheng J. Structural determination of Aβ25–35 micelles by molecular dynamics simulations. Biophys J. 2010; 99:666–674. [PubMed: 20643087]
50. D'Ursi AM, Armenante MR, Guerrini R, Salvadori S, Sorrentino G, Picone D. Solution structure of amyloid β-peptide (25–35) in different media. J Med Chem. 2004; 47:4231–4238. [PubMed: 15293994]
51. Wei GH, Jewett AI, Shea JE. Structural diversity of dimers of the Alzheimer amyloid-β(25–35) peptide and polymorphism of the resulting fibrils. Phys Chem Chem Phys. 2010; 12:3622–3629. [PubMed: 20336261]
52. Kittner M, Knecht V. Disordered versus fibril-like amyloid β(25–35) dimers in water: structure and thermodynamics. J Phys Chem B. 2010; 114:15288–15295. [PubMed: 20964446]
53. Kohno T, Kobayashi K, Maeda T, Sato K, Takashima A. Three-dimensional structures of the amyloid β peptide (25–35) in membrane-mimicking environment. Biochemistry. 1996; 35:16094–16104. [PubMed: 8973180]
54. Pike CJ, Walencewiczwasserman AJ, Kosmoski J, Cribbs DH, Glabe CG, Cotman CW. Structure-activity analyses of β-amyloid peptides - contributions of the β25–35 region to aggregation and neurotoxicity. J Neurochem. 1995; 64:253–265. [PubMed: 7798921]
55. Gessel MM, Bernstein S, Kemper M, Teplow DB, Bowers MT. Familial Alzheimer's disease mutations differentially alter amyloid β-protein oligomerization. ACS Chem Neurosci. 2012; 3:909–918. [PubMed: 23173071]

56. Bernstein SL, Wyttenbach T, Baumketner A, Shea JE, Bitan G, Teplow DB, Bowers MT. Amyloid β-protein: monomer structure and early aggregation states of Aβ42 and its Pro19 alloform. J Am Chem Soc. 2005; 127:2075–2084. [PubMed: 15713083]
57. Gessel MM, Wu C, Li H, Bitan G, Shea JE, Bowers MT. Aβ(39–42) modulates Aβ oligomerization but not fibril formation. Biochemistry. 2012; 51:108–117. [PubMed: 22129303]
58. Young LM, Saunders JC, Mahood RA, Revill CH, Foster RJ, Tu LH, Raleigh DP, Radford SE, Ashcroft AE. Screening and classifying small-molecule inhibitors of amyloid formation using ion mobility spectrometry-mass spectrometry. Nat Chem. 2015; 7:73–81. [PubMed: 25515893]
59. Lee S, Zheng XY, Krishnamoorthy J, Savelieff MG, Park HM, Brender JR, Kim JH, Derrick JS, Kochi A, Lee HJ, Kim C, Ramamoorthy A, et al. Rational design of a structural framework with potential use to develop chemical reagents that target and modulate multiple facets of Alzheimer's disease. J Am Chem Soc. 2014; 136:299–310. [PubMed: 24397771]
60. Soper MT, DeToma AS, Hyung SJ, Lim MH, Ruotolo BT. Amyloid-β-neuropeptide interactions assessed by ion mobility-mass spectrometry. Phys Chem Chem Phys. 2013; 15:8952–8961. [PubMed: 23612608]
61. Bleiholder C, Dupuis NF, Wyttenbach T, Bowers MT. Ion mobility-mass spectrometry reveals a conformational conversion from random assembly to β-sheet in amyloid fibril formation. Nat Chem. 2011; 3:172–177. [PubMed: 21258392]
62. Do TD, Economou NJ, LaPointe NE, Kincannon WM, Bleiholder C, Feinstein SC, Teplow DB, Buratto SK, Bowers MT. Factors that drive peptide assembly and fibril formation: experimental and theoretical analysis of Sup35 NNQQNY mutants. J Phys Chem B. 2013; 117:8436–8446. [PubMed: 23802812]
63. Do TD, Economou NJ, Chamas A, Buratto SK, Shea JE, Bowers MT. Interactions between amyloid-β and Tau fragments promote aberrant aggregates: implications for amyloid toxicity. J Phys Chem B. 2014; 118:11220–11230. [PubMed: 25153942]
64. Attar A, Bitan G. Disrupting self-assembly and toxicity of amyloidogenic protein oligomers by "molecular tweezers" - from the test tube to animal models. Curr Pharm Des. 2014; 20:2469–2483. [PubMed: 23859557]
65. Acharya S, Safaie BM, Wongkongkathep P, Ivanova MI, Attar A, Klarner FG, Schrader T, Loo JA, Bitan G, Lapidus LJ. Molecular basis for preventing α-synuclein aggregation by a molecular tweezer. J Biol Chem. 2014; 289:10727–10737. [PubMed: 24567327]
66. Luhrs T, Ritter C, Adrian M, Riek-Loher D, Bohrmann B, Doeli H, Schubert D, Riek R. 3D structure of Alzheimer's amyloid-β(1–42) fibrils. Proc Natl Acad Sci U S A. 2005; 102:17342–17347. [PubMed: 16293696]
67. Petkova AT, Ishii Y, Balbach JJ, Antzutkin ON, Leapman RD, Delaglio F, Tycko R. A structural model for Alzheimer's β-amyloid fibrils based on experimental constraints from solid state NMR. Proc Natl Acad Sci USA. 2002; 99:16742–16747. [PubMed: 12481027]
68. Balbach JJ, Ishii Y, Antzutkin ON, Leapman RD, Rizzo NW, Dyda F, Reed J, Tycko R. Amyloid fibril formation by Aβ16–22, a seven-residue fragment of the Alzheimer's beta-amyloid peptide, and structural characterization by solid state NMR. Biochemistry. 2000; 39:13748–13759. [PubMed: 11076514]
69. Wyttenbach T, Kemper PR, Bowers MT. Design of a new electrospray ion mobility mass spectrometer. Int J Mass Spectrom. 2001; 212:13–23.
70. Bleiholder C, Wyttenbach T, Bowers MT. A novel projection approximation algorithm for the fast and accurate computation of molecular collision cross sections (I). Method. Int J Mass Spectrom. 2011; 308:1–10.
71. Bleiholder C, Contreras S, Do TD, Bowers MT. A novel projection approximation algorithm for the fast and accurate computation of molecular collision cross sections (II). Parameterization and application to biomolecules. Int J Mass Spectrom. 2013; 345–347:89–96.

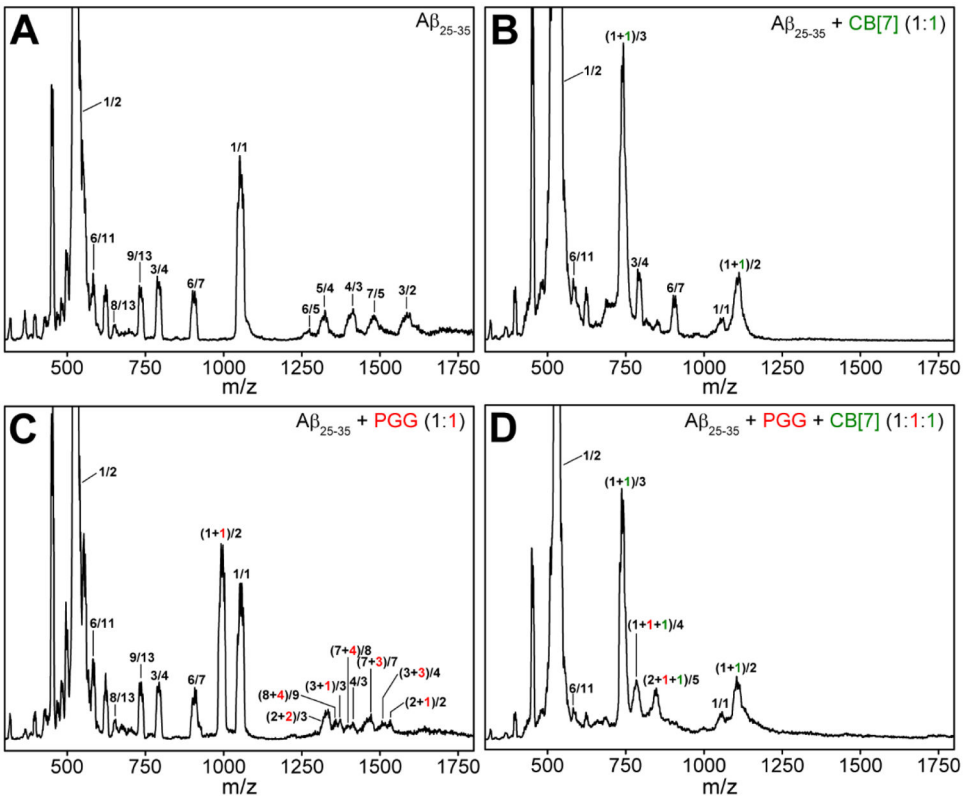

Figure 1.

ESI-Q mass spectra of (A) pure A$\beta_{25–35}$, (B) A$\beta_{25–35}$ incubated with CB[7] at 1:1, (C) A$\beta_{25–35}$ incubated with PGG at 1:1, and (D) A$\beta_{25–35}$ incubated with PGG and CB[7] at 1:1:1 molar ratio. The A$\beta_{25–35}$ concentration was 100 μM in acidified water (0.1% (v/v) of formic acid) in all cases. The peaks of the A$\beta_{25–35}$ homo-oligomers are annotated as ratios of the oligomer size *n* and the charge *z*, whereas the hetero-oligomer peaks of A$\beta_{25–35}$ with ligands are annotated by $(n+p)/z$, $(n+k)/z$ and $(n+p+k)/z$ where *p* and *k* are the numbers of PGG and CB[7] molecules, respectively.

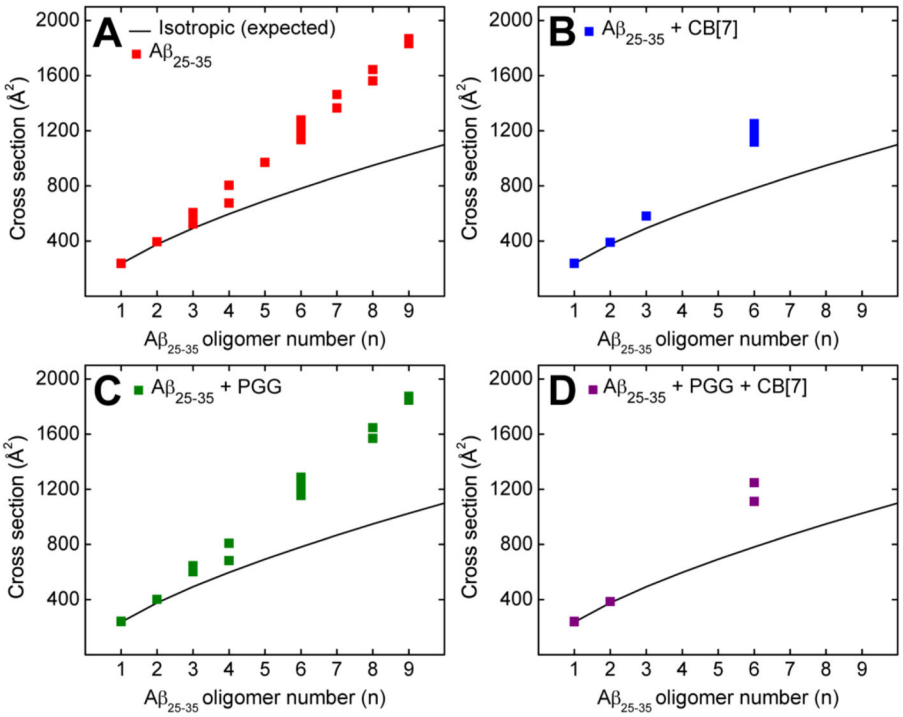

Figure 2.

Oligomer growth curve data of the A$\beta_{25–35}$ homo-oligomers of (A) pure A$\beta_{25–35}$, (B) A$\beta_{25–35}$ incubated with CB[7] at 1:1, (C) A$\beta_{25–35}$ incubated with PGG at 1:1, and (D) A$\beta_{25–35}$ incubated with PGG and CB[7] at 1:1:1 molar ratio.

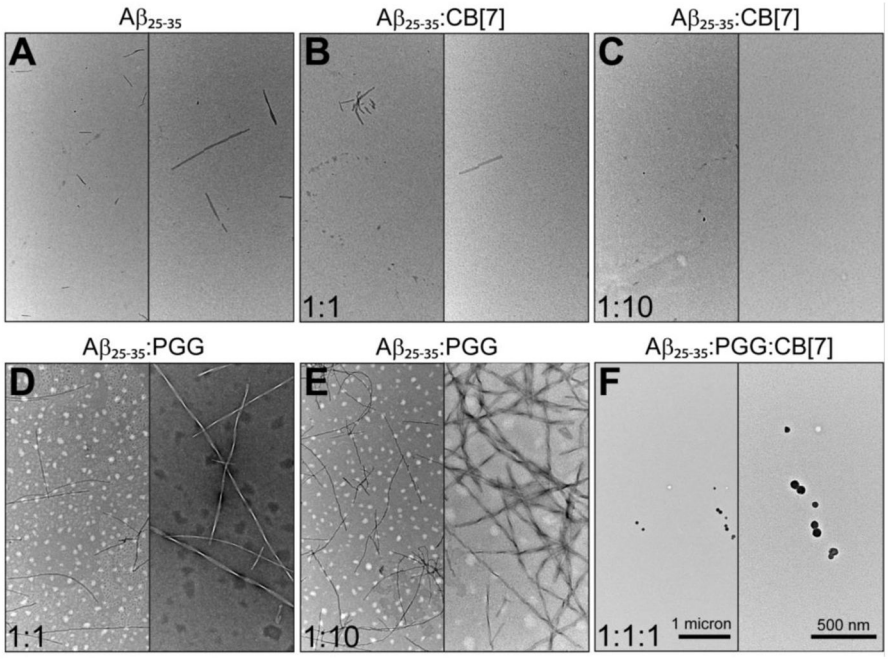

Figure 3.

Representative TEM images of (A) pure A$\beta_{25–35}$, (B, C) A$\beta_{25–35}$ incubated with CB[7] at 1:1 and 1:10, (D, E) A$\beta_{25–35}$ incubated with PGG at 1:1 and 1:10, and (F) A$\beta_{25–35}$ incubated with PGG and CB[7] at 1:1:1 molar ratio. The scale bars for all images are given in the two panels of section F.

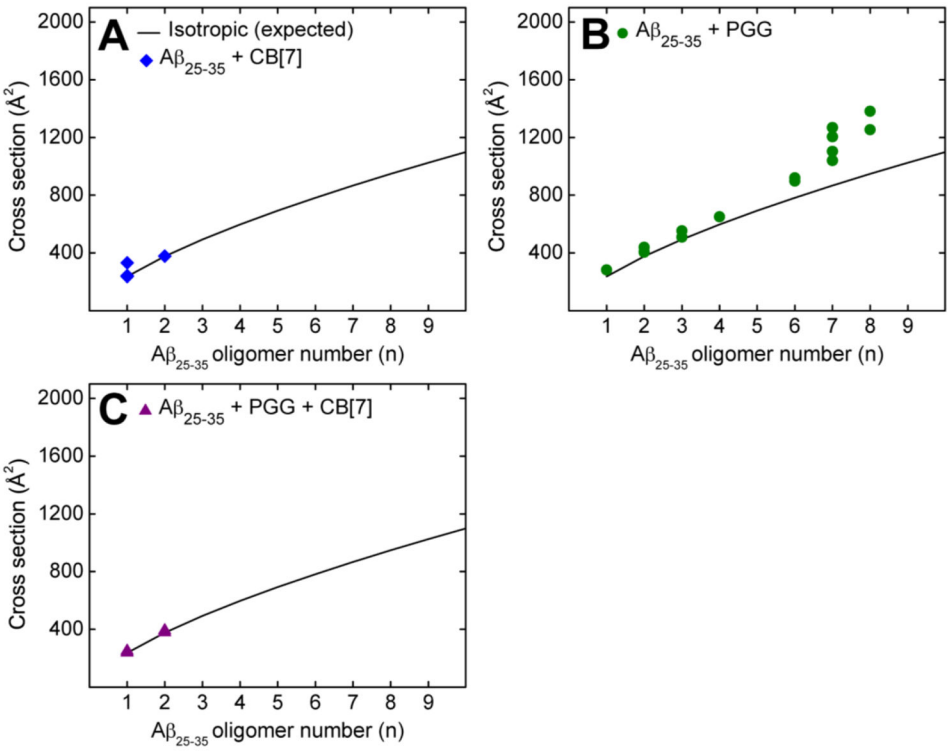

Figure 4.

Oligomer growth curve data of hetero-oligomers of (A) A$\beta_{25–35}$ incubated with CB[7] at 1:1, (B) A$\beta_{25–35}$ incubated with PGG at 1:1, and (C) A$\beta_{25–35}$ incubated with PGG and CB[7] at 1:1:1 molar ratio. The cross sections of A$\beta_{25–35}$ oligomers reported here were extracted from the hetero-oligomer cross sections (see Supporting Information Tables S2, S3 and S4).

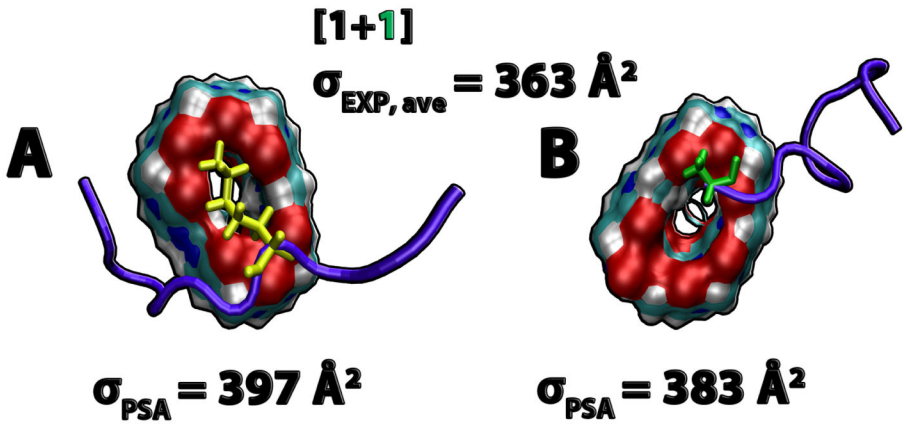

Figure 5.

Representative structures of A$\beta_{25–35}$:CB[7] complexes obtained from simulations. (1+1) complexes extracted from the simulation, and their theoretical cross sections. The experimental cross section is an average of the (1+1)/2 and (1+1)/3 complexes. The CB[7] molecules are represented in filled surface with oxygens in red, carbons in cyan, nitrogens in blue and hydrogens in white. The A$\beta_{25–35}$ peptides are shown in cartoon representation and colored in violet. Lysine (yellow) and N-terminus (green) are shown in licorice representation.

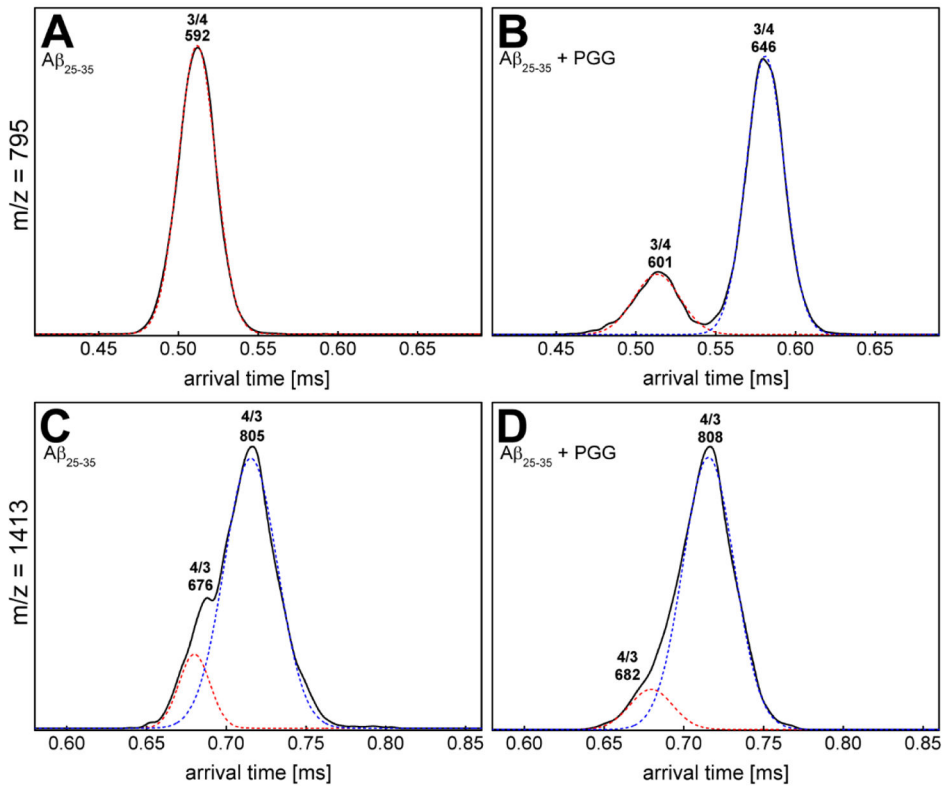

Figure 6.

Representative arrival time distributions (ATDs) for *m*/*z* = 795 and *m*/*z* = 1413 of (A, C) pure A$\beta_{25–35}$ and (B, D) A$\beta_{25–35}$ incubated with PGG at 1:1 molar ratio.

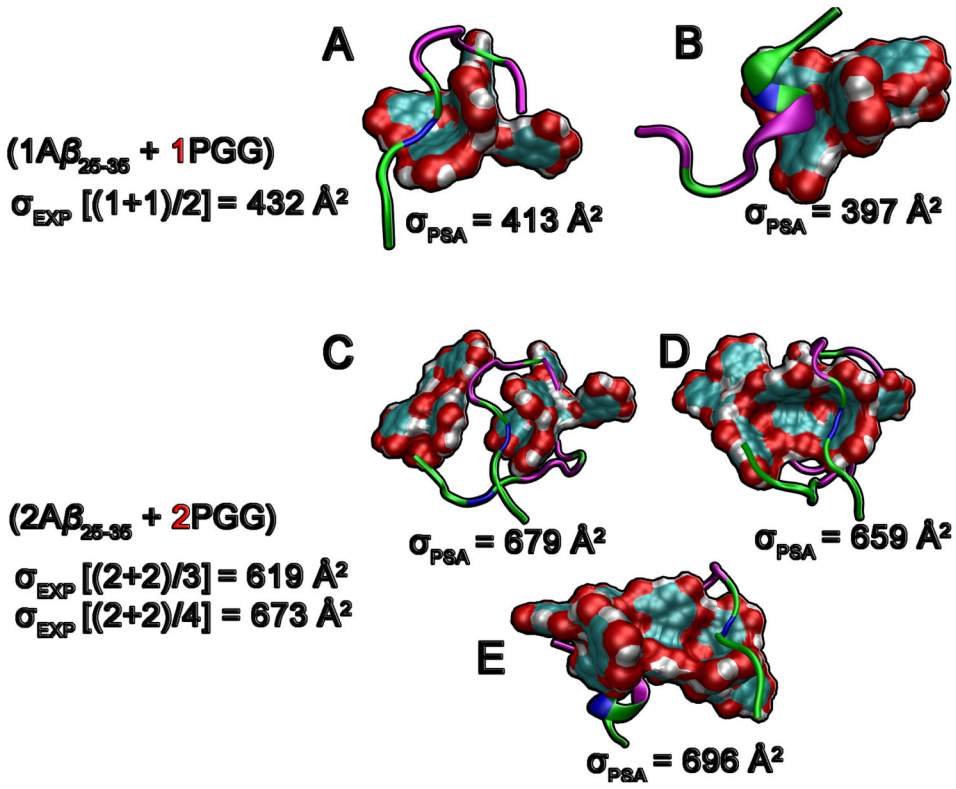

Figure 7.

Representative structures of A$\beta_{25–35}$:PGG complexes obtained from simulations. (A, B) Hetero-dimers of one A$\beta_{25–35}$ and one PGG. A$\beta_{25–35}$ monomers adopt a wide range of structures from random coil to partial helix. (C, D, E) Hetero-tetramers of two A$\beta_{25–35}$ and two PGG molecules. The PGG molecules are represented in filled surface with oxygens in red, carbon in cyan and hydrogen in white. The A$\beta_{25–35}$ peptides are shown in cartoon representation where non-polar residues are shown in pink, charged residues in blue and polar residues in green.

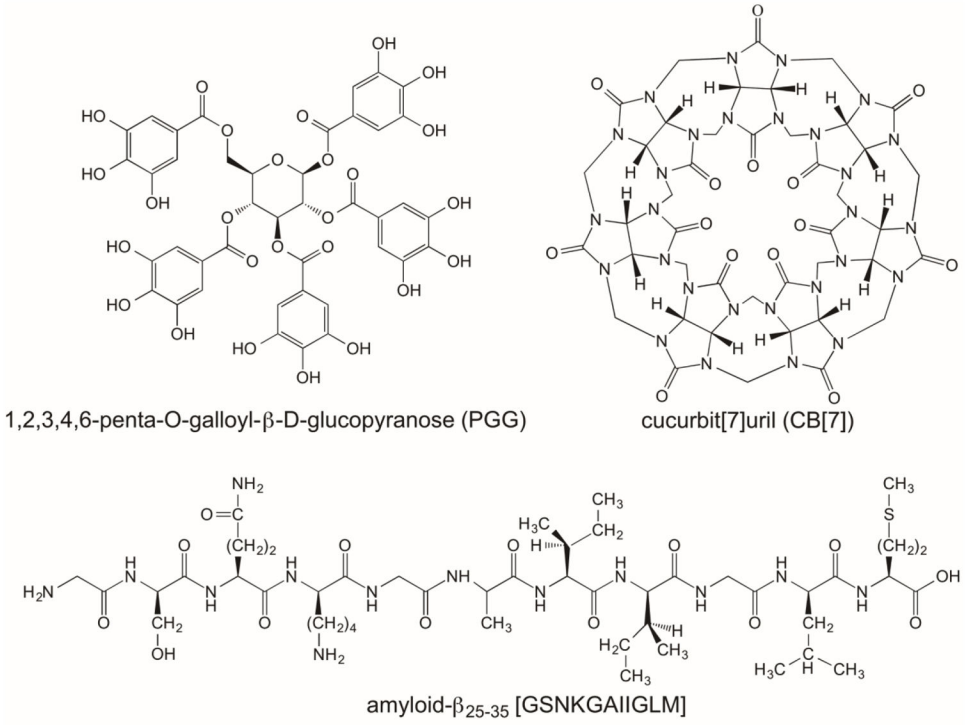

Scheme 1.

Structural formulas of 1,2,3,4,6-penta-O-galloyl-β-D-glucopyranose (PGG), cucurbit[7]uril (CB[7]) and A$\beta_{25–35}$.